



Aerodynamic and Aeroacoustics Predictions of Wells Turbines Using LBM

Mohammed Meskine¹, Franck Pérot², Min-Suk Kim³, Adrien Mann⁴
Exa Corporation, Brisbane, CA, 94005, USA

Ralf Starzmann⁵, Thomas Carolus⁶
UNIVERSITY OF SIEGEN, Institute for Fluid- and Thermodynamics, Paul-Bonatz-Strasse 9-11, D-57068 Siegen, GERMANY

Oscillating Water Column (OWC) power plant is another form of “green energy” sources. It converts the motion of water waves into a bi-directional air flow which then drives an air turbine. The Wells Turbine, as a candidate for OWC power take off systems, was the object of considerable researches during the last decades. Optimization of aerodynamic performances reduction of noise generation is crucial for Wells Turbines to achieve great efficiency and meet acoustic regulations. The use of digital methods during the development process is then the way to avoid expensive prototypes and to optimize the OWC. In this paper, an unsteady and compressible computational approach based on the Lattice Boltzmann Method is used to simultaneously predict the 3-D turbulent flow and the corresponding acoustic field of a scaled model of the Wells Turbine. This scaled turbine was developed and intensively studied at Siegen University in Germany. The existing experimental aerodynamic and acoustic are first used to validate the numerical approach. In turn, the numerical results are used to investigate the origin of the noise as they provide insight on the link between flow structures and noise generation.

I. Introduction

A Wells Turbine is an axial turbine, capable of extracting energy from the oscillating airflow generated by the motion of water waves. The Wells Turbine is therefore operating along its complete characteristic curve from no load to overload and reversely. Consequently, it is important to maximize its performances at both forward and backward cycles via the optimization of the blades shape design and of its position inside the OWC plant. Radiated noise levels are also crucial parameters to be taken into account when designing a turbine for a OWC system in order to guarantee the acoustic comfort of people working on site or living in the surrounding area. Many studies have been performed during the past decades. However, this study will focus on intensive experimental investigations which were performed using a scaled model turbine at Siegen University¹⁻⁵.

The main goal of the present work is to validate a digital solution for predicting the aerodynamic and aeroacoustic performances of a Wells Turbine which can then be used as an alternative to prototyping and time-consuming experiments, not always easy to carry-on. Transient and compressible CFD (Computational Fluid Dynamics) simulations are performed on the digital scaled model turbine provided by Siegen University. The turbine rotation is truly reproduced at the real rotation speed and the self induced noise is directly recovered from the compressible CFD/CAA (Computational AeroAcoustics) simulations. The aerodynamic performance of the Wells Turbine, in term of pressure drop as a function of mass flow, is analyzed and compared to experiments. Direct noise prediction is also compared to Siegen University test results for two operating points and two tip clearances. In a first section,

¹ Principal Aeroacoustics Engineer, mmeskine@exa.com

² Senior Director, Aeroacoustic Application Management, perot@exa.com

³ Principal Aeroacoustics Engineer, mskim@exa.com

⁴ Senior Aeroacoustic Engineer, amann@exa.com

⁵ Professor Fluid Engineering, thomas.carolus@uni-siegen.de

⁶ Dr. Mechanical Engineer, RStarzmann@schottel.de

the experiments are summarized and the numerical aspects, namely the simulation method, the computational domain and the numerical conditions are described. In a second part, the predicted aerodynamic performances are analyzed and compared to experiments. Direct noise prediction and unsteady flow analysis are performed in the last section in order to highlight the link between Wall Pressure Fluctuations (WPF) and radiated acoustics intensity.

II. Experimental and numerical setups

A. Experimental setup

1. Test Facility description

A unidirectional, steady state test rig is used for this study, as depicted in Figure 1. The turbine rotor is mounted in a cylindrical annular duct. The variable but steady volume flow rate is supplied by a centrifugal fan (c) with a variable speed drive. The plenum (e) contains screens and honeycombs (f) used as flow straighteners upstream a calibrated nozzle (g). Another honeycomb (j) is located directly upstream of the turbine section (k). The rotor torque is measured via an integral telemetric torque flange, which in turn is mounted on a water cooled synchronous motor-generator system with variable speed drive. For the acoustic tests, the rig is equipped with highly efficient silencers (a), (b) and (d) around the air supply.

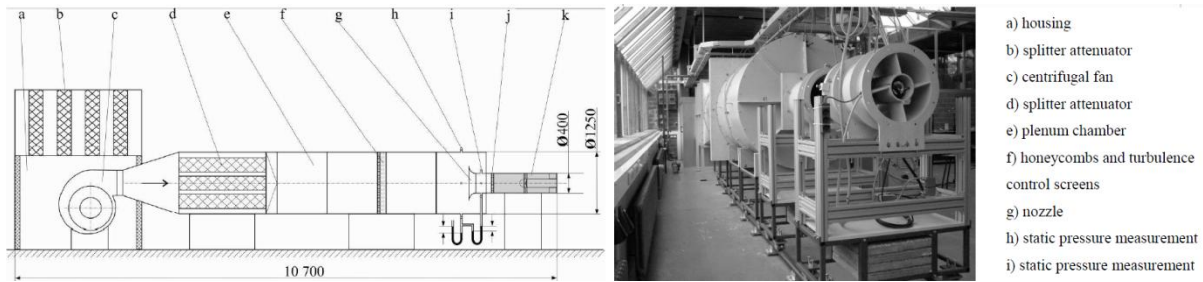


Figure 1: Test facility

2. Aerodynamic performance tests

The aerodynamic experiments in this study are carried out with a constant rotor speed of $n = 4000 \text{ rpm}$. The pressure in the plenum chamber and the flow rate are increased from zero to a point beyond stall and then decreased back to zero. A control and data acquisition system is used to collect instantaneous data for each point of operation. For each flow rate Q , the pressure rise in the plenum ΔP and the torque T are provided. Based on the specified accuracy of the instruments, the uncertainty for each data point is within a range of $\pm 5 \%$. Note that the repeatability of the experiments was within a range of $\pm 2 \%$ for each data point.

3. Acoustic tests

Acoustic and aerodynamic measurements are carried out simultaneously. The result is an acoustic characteristic curve presenting the overall sound pressure level for each operating point. Due to the very efficient acoustic absorbers in the in- and outlet of the pressurized air supply, no correction for background noise is required. However, no acoustic treatment is applied to the test facility walls which may leads to acoustic reflections from the ceiling and from the rest of the test facility components. A Brüel & Kjaer RSS (type 4204) microphone is used in all experiments to measure sound pressure level L_p at 3m from the duct exit (see Figure 2). Time pressure signals were recorded at a sampling rate of 25,600Hz for a total time of 5 sec.

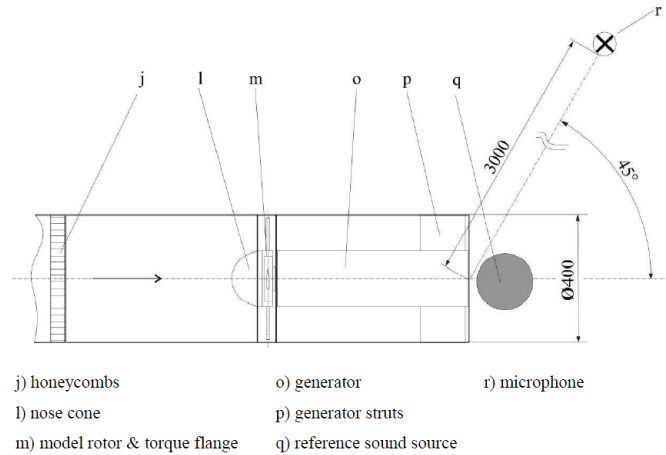


Figure 2: Turbine section schematic view and microphone position

4. Turbine model description

The turbine rotor used in this study is mounted in a cylindrical annular duct of diameter $D_{tip} = 400$ mm diameter. Various geometry parameters are experimentally investigated:

- Tip ratios (r_{hub}/r_{tip}) from 0.43 to 0.6,
- NACA airfoil profile,
- Tip clearance ratio Δ/D_{tip} from 0.175 to 1.71%
- ...

However, the turbine model used for numerical simulation is limited to the following variations:

- Tip ratio of 0.43
- Five blades,
- Two different tip clearance ratios 0.175 and 1.71% corresponding respectively to 0.7 mm and 6.8 mm of tip clearance.

The corresponding rotor design is presented in Figure 3 with indication of the rotation direction.

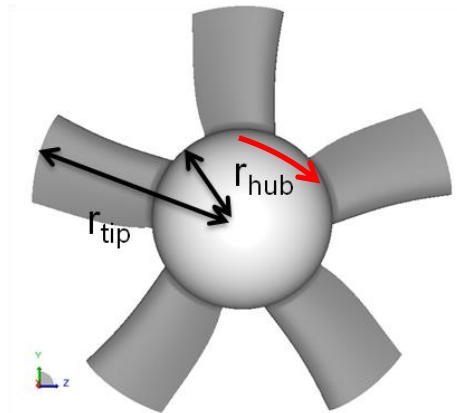


Figure 3: Studied blade design (front view)

B. Numerical setup

1. Lattice Boltzmann Method

The CFD/CAA code PowerFLOW 5.0 is used to compute simultaneously the turbulent flow and the corresponding acoustic radiation. The code is based on the Lattice Boltzmann Method (LBM). Lattice based methods were proposed a couple of decades ago⁶⁻¹¹ as an alternative numerical method to traditional Computational Fluid Dynamics (CFD). Unlike conventional methods based on discretizing the macroscopic continuum equations,

LBM starts from “mesoscopic” kinetic equations, i.e. the Boltzmann equation, to predict macroscopic fluid dynamics. The lattice Boltzmann equation has the following form:

$$f_i(\vec{x} + \vec{c}_i \Delta t, t + \Delta t) - f_i(\vec{x}, t) = C_i(\vec{x}, t) \quad (1)$$

where f_i is the particle distribution function moving in the i^{th} direction, according to a finite set of the discrete velocity vectors $\{c_i; i=0, \dots, b\}$, $c_i \Delta t$ and Δt are respectively space and time increments. For convenience, we choose the convention $\Delta t=1$ in the following discussions. The collision term on the right hand side of equation 1 adopts the simplest and most popular form known as the Bhatnagar-Gross-Krook (BGK) form¹²⁻¹⁶:

$$C_i(\vec{x}, t) = -\frac{1}{\tau} [f_i(\vec{x}, t) - f_i^{eq}(\vec{x}, t)] \quad (2)$$

Here τ is the relaxation time parameter, and f_{ieq} is the local equilibrium distribution function, which depends on local hydrodynamic properties. The basic hydrodynamic quantities, such as fluid density ρ and velocity u , are obtained through moment summations:

$$\rho(\vec{x}, t) = \sum_i f_i(\vec{x}, t), \quad \rho \vec{u}(\vec{x}, t) = \sum_i \vec{c}_i f_i(\vec{x}, t) \quad (3)$$

In the low frequency and long-wave-length limit, for a suitable choice of the set of discrete velocity vectors, the transient compressible Navier-Stokes equations are recovered through Chapman-Enskog expansion, in the limit of low Mach numbers ($M \sim 0.4$). The resulting equation of state obeys the ideal gas law, and the kinematic viscosity of the fluid is related to the relaxation time parameter τ as shown for instance by Shan and Chen¹⁷:

$$\nu = (\tau - 1/2)l \quad (4)$$

The combination of equations 1 to 4 forms the usual LBM scheme for fluid dynamics. It is solved on a grid composed of cubic volumetric elements called voxels, and a Variable Resolution (VR) strategy is allowed, where the grid size changes by a factor of two for adjacent resolution regions¹⁸.

In order to model the effects of unresolved small scale turbulent fluctuations, the lattice Boltzmann equation is extended by replacing its molecular relaxation time scale with an effective turbulent relaxation time scale, i.e. $\tau \rightarrow \tau_{eff}$, where τ_{eff} is derived from a systematic Renormalization Group (RG) procedure detailed by Chen et al.^{19,20}. This method is commonly called Very Large Eddy Simulation (VLES) and is now validated and productively used for solving a large range of problems such as aerodynamics, thermal, aerospace and aeroacoustics²¹⁻²⁷.

2. Geometry and numerical aspect

The simulated geometry presented in Figure 4 is a digital Wells Turbine scaled model enclosed by a cylindrical annular duct of 400 mm diameter. The duct is extended by 4 m upstream the turbine in order to ensure a numerical anechoic termination. The geometry is embedded into a large anechoic simulation domain with dimensions 26x26x15m³. The finest grid resolution used around the rotor is $\Delta x=0.25$ mm corresponding to 1600 voxels across the turbine diameter. Two boundary conditions are used:

- Inlet mass flow imposed at the duct inlet,
- Constant rotor speed rotation 4000 rpm.

The simulation time step is $dt=4.12 \times 10^{-7}$ s and the calculation is performed over a period $T=0.15$ s of physical time corresponding to 10 complete turbine rotations. The resolution at the far-field microphones (3m from duct exit) is $\Delta x_{mic}=8$ mm and assuming 16 points per wave length are necessary to propagate acoustics waves with minimum dissipation, the estimated grid cut-off frequency is $f_{cut} \sim 3000$ Hz. To perform the unsteady flow analyses, the instantaneous pressure and velocity components are recorded on various surfaces and volumes at a high frequency rate for three rotations.

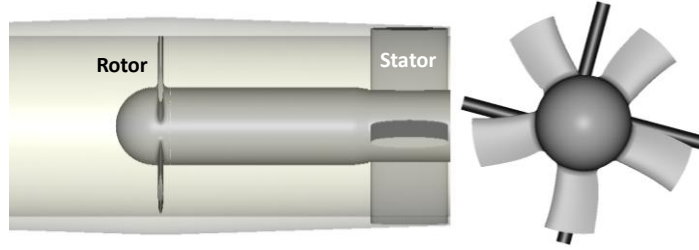


Figure 4: Simulated Wells Turbine geometry

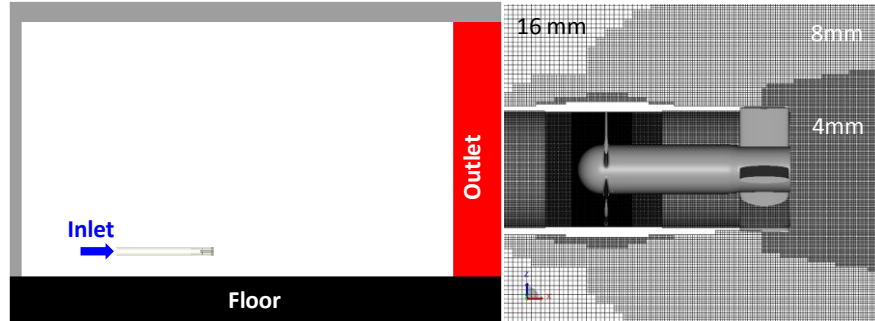


Figure 5: Numerical wind tunnel (left) and grid overview (right)

3. Simulated configurations

The focus of the present study, as a first step, is the pre-stall regime of the Wells Turbine model. Four simulations are performed. The characteristics of each configuration are summarized in table 1. The stall regime may be presented in the future as an extension to the present work.

Simulation	Flow Rate [m ³ /s]	Tip clearance ratio Δ/D_{tip}
1	$Q_1 = 0.9966$	$t_{c1} = 0.175 \%$
2	$Q_2 = 1.481$	$t_{c1} = 0.175 \%$
3	$Q_1 = 0.9966$	$t_{c2} = 1.71 \%$
4	$Q_2 = 1.481$	$t_{c2} = 1.71 \%$

Table 1: Simulations list

III. Aerodynamic performance analysis

A. Pressure drop and torque analysis

The turbine performance curves are presented in Figure 6. The numerical curve in blue is obtained by performing two simulations at two different flow rates Q_1 and Q_2 using tip clearance ratios t_{c1} and t_{c2} . After 5 rotor rotations, the pressure P_I inside the duct is converged and the pressure drop $P = P_I - P_0$ is derived. The comparison with the measurement gives very satisfying agreement with a maximum error in pressure drop of 4% which is within the uncertainty of the experimental measurement ($\pm 5\%$).

The torque is also well predicted with a maximum delta of 4.1% from experiments. The stall regime, according to the experimental results, occurs around 2.05 m³/s. The stall effect in the pressure drop curve is presented by a step while an important drop in torque is observed.

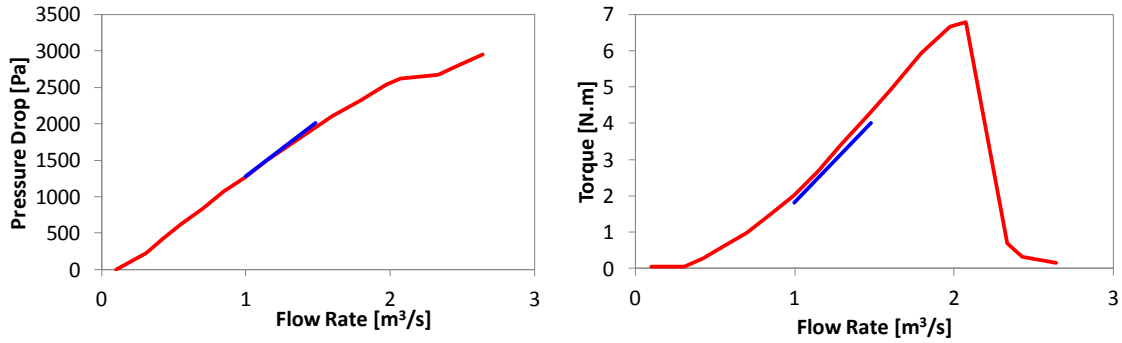


Figure 6: Turbine performances curves with using t_{c1} ; (left) pressure drop; (right) torque; (—) experiment; (—) simulation

The analysis of the surface streamlines and average pressure coefficient C_p field in both suction and pressure sides are presented in Figure 7. The flow is totally attached on the pressure side for both flow rates. However, the suction side shows a significant flow detachment for both flow rates.

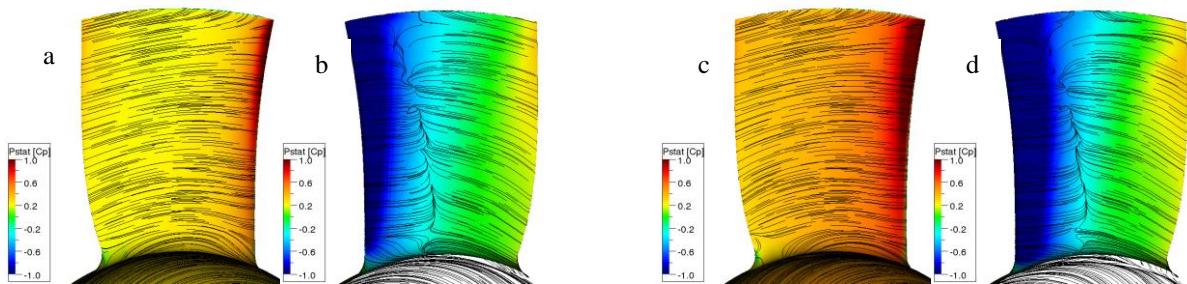


Figure 7: Averaged C_p and surface streamlines on pressure side (a and c) and suction side (b and d) using t_{c1} for Q_1 (left) and Q_2 (right)

B. Tip clearance effect on aerodynamic performance

Two additional simulations using tip clearance ratio t_{c2} are investigated in this section. Pressure drop and torque predictions are compared to experimental data in Figure 8. Similarly to the results obtained with t_{c1} , the second tip clearance results are in very good agreement with experiments. The new operating points are still in pre-stall regime. However, the stall regime with t_{c2} is delayed from 2 to approximately 2.5 m^3/s .

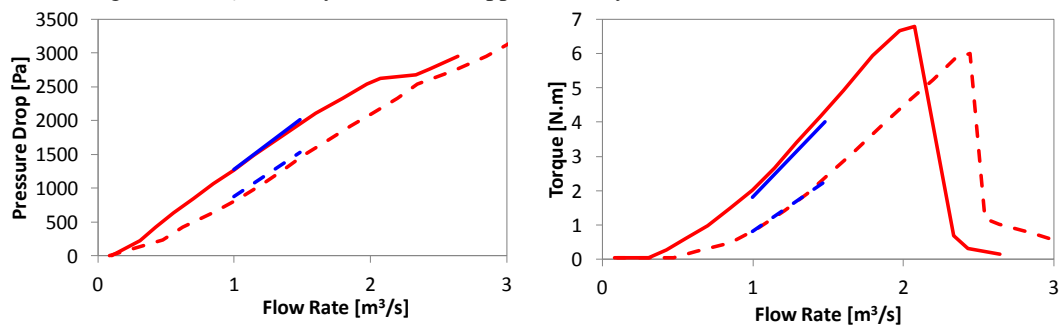


Figure 8: (Left) turbine performance curves;(right) torque curves; (solid line) t_{c1} ; (dash line) t_{c2} ; (—) experiment; (—) simulation;

Figure 9 shows the average C_p and streamlines comparison for all configurations. Increasing the tip clearance leads to lower pressure on the pressure side. Additional flow is leaking through the tip clearance and tip vortex clearly appears at both operating points.

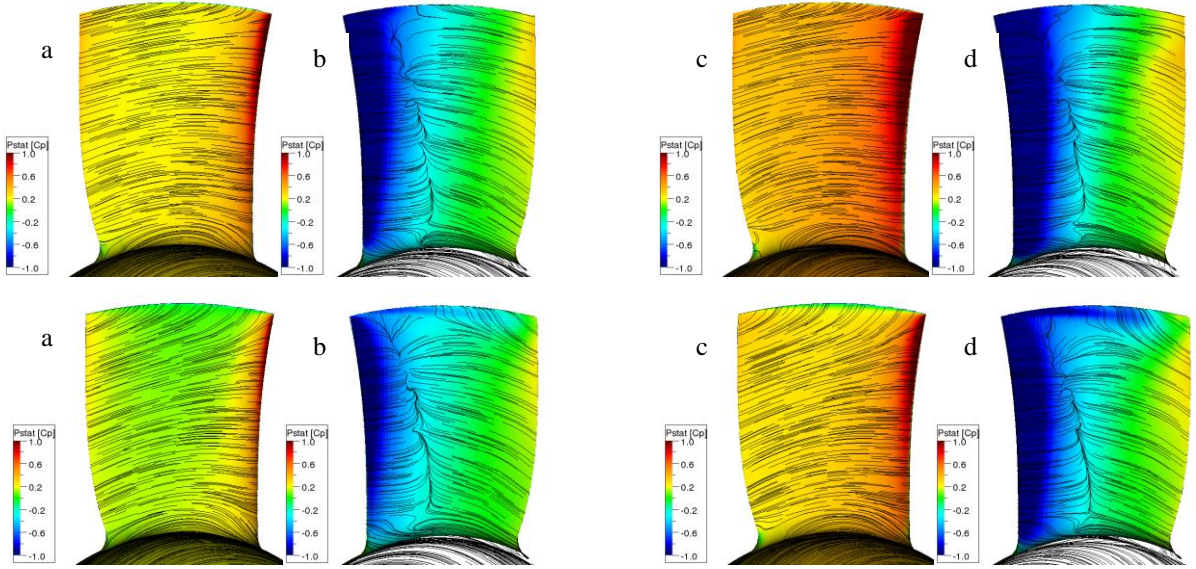


Figure 9: Averaged Cp and surface streamlines on pressure side (a and c) and suction side (b and d). (left) Q_1 ; (right) Q_2 . (top) t_{c1} ; (bottom) t_{c2}

IV. Acoustic performance analysis

A. Acoustic performance predictions

Figure 10 shows the overall sound pressure level comparison, for the frequency range [200, 3000Hz], between simulation and experiments, using tip clearance ratio t_{c1} . For both flow rates, the maximum prediction error is less than 1dBA. Increasing the flow rate from 0.997 to 1.481 m^3/s contributes then to increase the OASPL by 5dB in both experiments and simulations.

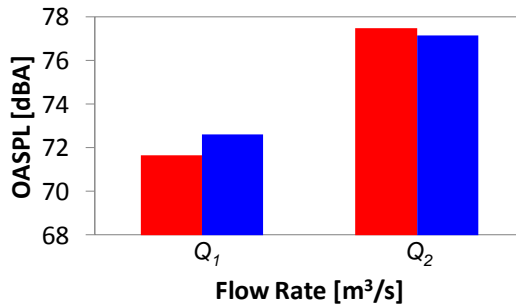


Figure 10: OASPL comparison for $f \in [200; 3000 \text{ Hz}]$ using t_{c1} ; (—) experiments; (—) simulation

In Figure 11, the predicted SPL is compared to the experiments for both flow rates. A good agreement is observed. However, the dB levels are underestimated for frequencies above 2000Hz for both flow rates which may occur from:

- Numerical coarse resolution at the microphone position (8mm).
- Absence of acoustic treatment of the walls on the experimental test facility.

Figure 12 shows a significant noise increase with higher flow rate especially at high frequencies. The noise levels increase induced by higher flow rate is correctly predicted by the simulation since a good agreement with experiments is observed.

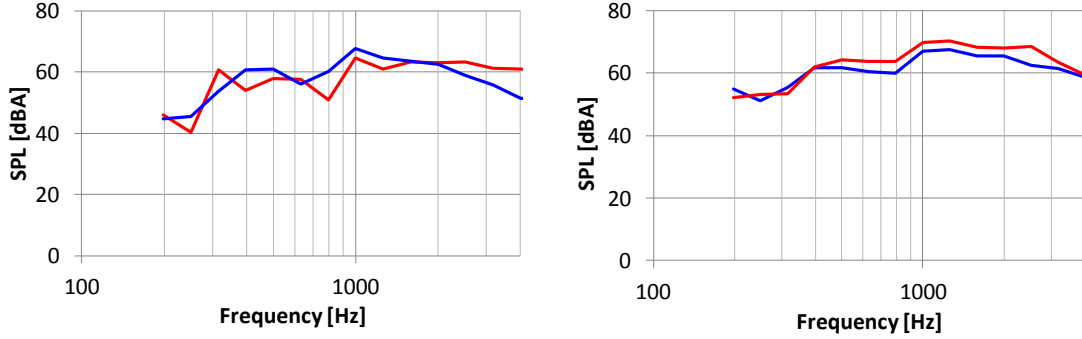


Figure 11: SPL comparison for Q_1 (left) and Q_2 (right) using t_{c1} ; (—) experiments; (—) simulation

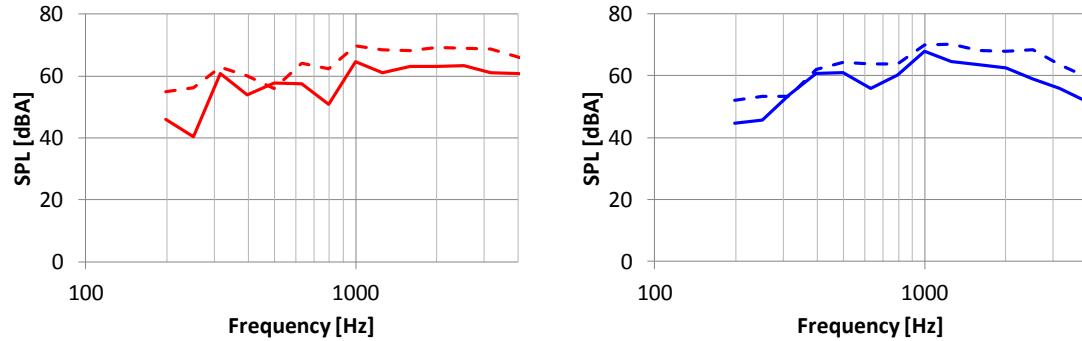


Figure 12: SPL comparison; (—) experiments (—) simulation; (solid line) Q_1 ; (dash line) Q_2

B. Tip clearance effect

As mentioned previously, the experimental SPL using tip clearance ratio t_{c1} was not provided. Therefore, a pure numerical investigation of the tip clearance effect on noise is presented in this section. Figure 13 shows:

- Very small effect on OASPL (less than 0.5dB) at the optimum flow rate.
- 3 dB of noise reduction at the flow rate Q_2 .

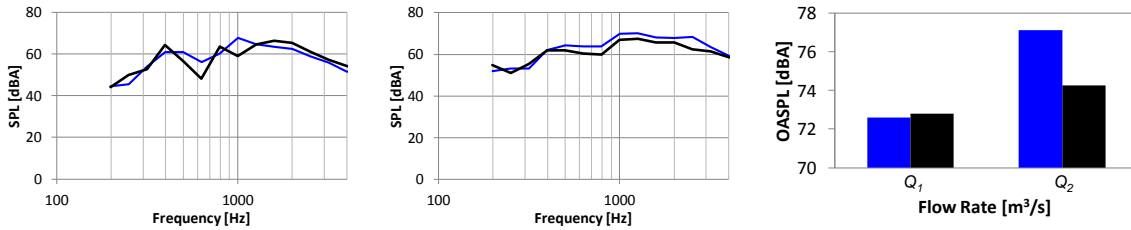


Figure 13: SPL and OASPL comparison for t_{c1} (—) and t_{c2} (—); (left) Q_1 ; (middle) Q_2 ; (right) OASPL for $f \in [200; 3000\text{Hz}]$

V. Unsteady flow analysis

In the following section, the flow is analyzed in time and frequency. The goal is to highlight numerically the existing link between wall pressure fluctuations and radiated acoustics. A better understanding of the effect of the flow rate and tip clearance on radiated noise is also expected.

A. Flow rate effect analysis

1. Instantaneous flow

Figure 14 shows velocity and vorticity magnitude in the vertical symmetry plane for both flow rates. It is obvious that higher flow rate leads to higher intensity flow structures especially close to the rotor. In Figure 15, a flow detachment on the suction side is better observed and is mainly located in the blade/hub region. At higher flow rate, this detachment is present on a larger portion of the blade and seems more intense. It is thus a likely candidate

for higher noise generation levels. The tip vortex is also predicted at both flow rates and no interaction with the other blades is observed here. However, the high flow rate tip vortex is more intense while less coherent. Such reduced coherence, i.e multiple high intensity vortices, is likely related to an increase in the noise generation levels.

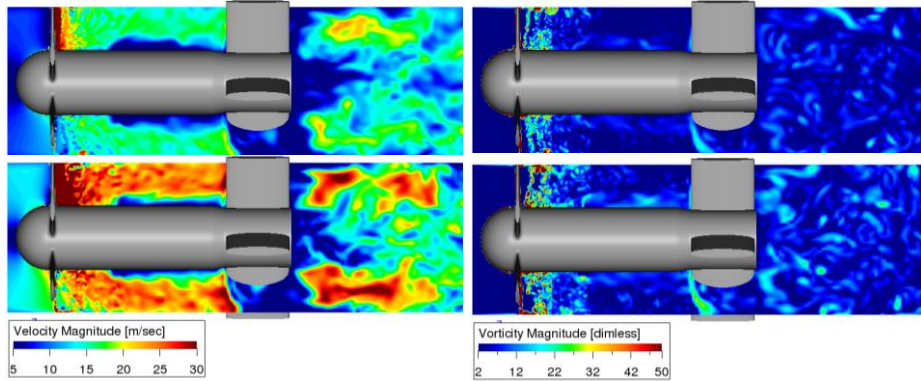


Figure 14: Instantaneous velocity magnitude (left) and vorticity magnitude (right); (top) Q_1 ; (bottom) Q_2

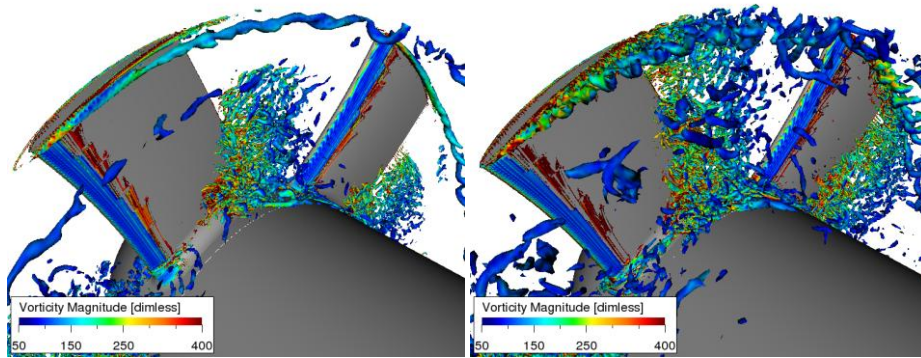


Figure 15: Instantaneous Isosurface of λ_2 colored by vorticity magnitude; (left) Q_1 ; (right) Q_2

2. Spectral analysis

Figure 16 shows the wall pressure fluctuations on the suction side of the rotor. At flow rate Q_2 , the higher wall-pressure fluctuations observed in the blades tip area indicate a strong noise generation at high frequencies. It thus illustrates the increasing effect on noise generation of tip vortices with higher flow rate. This last statement provides a direct link to the increase of the SPL observed in Figure 12. Similarly, the flow detachment in the blade/hub region generates higher wall pressure fluctuations for all frequencies with Q_2 .

Figure 17 shows the wall pressure fluctuations on the rotor for both pressure and suction sides. On the pressure side, the flow is completely attached for both flow rates. Since no flow detachment is present, the high dB levels on the pressure side are only related to the acoustic pressure radiated from the suction side. We can then highlight a major noise source located in the blades/hub region for both Q_1 and Q_2 configurations. An additional noise source related to the tip vortex is observed in the tip clearance area for Q_2 configuration only. It confirms the earlier observation on the strong incoherent structure observed at higher flow rate and directly identifies the location of the noise sources.

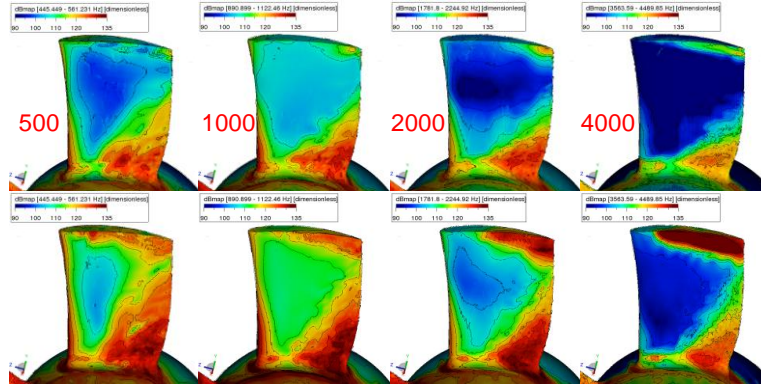


Figure 16: Surface dBMaps on suction side for frequencies 500 to 4000Hz; (top) Q_1 ; (bottom) Q_2

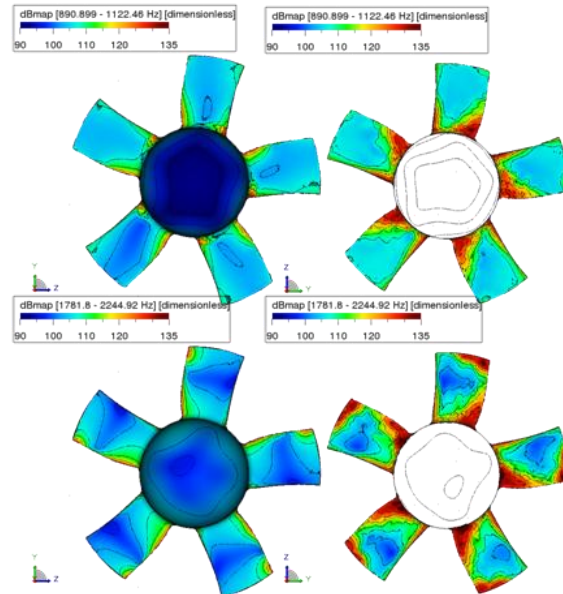


Figure 17: 1000Hz surface dBMaps for pressure side (left) and suction side (right); (top) Q_1 ; (bottom) Q_2

Figure 18 shows the SPL spectrogram using Q_2 and t_{cl} results. For each spectrogram, five surface microphones are used (one on each blade). The dB levels are then plotted for each blade and for each third octave band. The microphones are located on 12 different positions on the blade. The interest of such analysis is to check in the frequency domain the effect of the flow behavior on each blade. If the behavior is varying between the blades, it would indicate a possible rotation stall. Otherwise it will contribute for a better understanding of the noise sources identification.

In this section, SPL spectrogram analysis is used to enforce what was observed using the wall pressure fluctuations in Figure 16. Twelve microphones are used in the suction side; four for each blade section. The surface microphones “A” are located in the leading edge. Microphones “D” are close to the flow detachment and finally microphones “H” are located on the trailing edge. Similarly to the wall pressure fluctuations analysis, the SPL spectrograms confirm the conclusions made before:

- Low frequencies noise component mainly controlled by the flow detachment on the suction side (Microphones position 2),
- High frequencies noise component related to the tip vortex (microphones position 7).

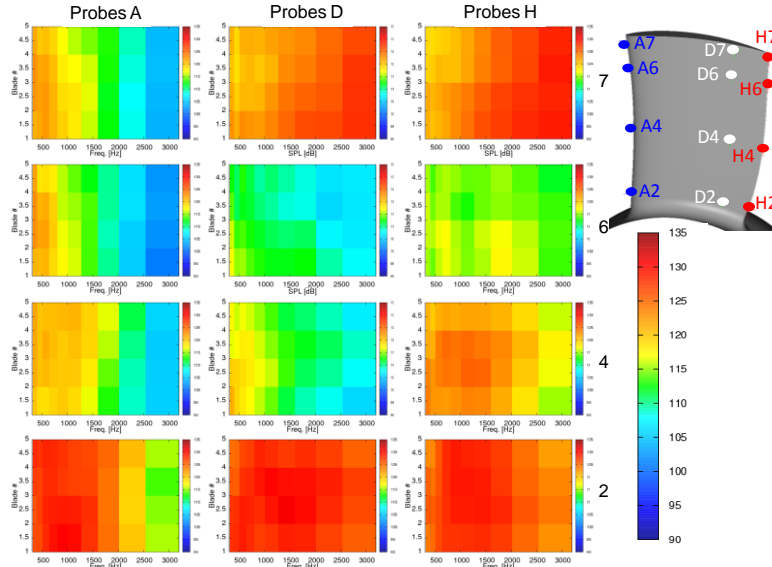


Figure 18: (left) SPL spectrogram for 12 microphones; (right) Microphones position

In Figure 19, the acoustic waves radiated from the Wells Turbine at flow rate Q_1 and Q_2 are presented using the instantaneous dilatation field. As expected, the acoustic levels are clearly higher, especially for shorter wavelengths corresponding to the higher frequency fluctuations mainly observed at the blades tip. It confirms that the tip vortex noise becomes dominant at higher flow rate since the blade suction side fluctuations increase with flow rate is not as obvious as observed in Figure 16.

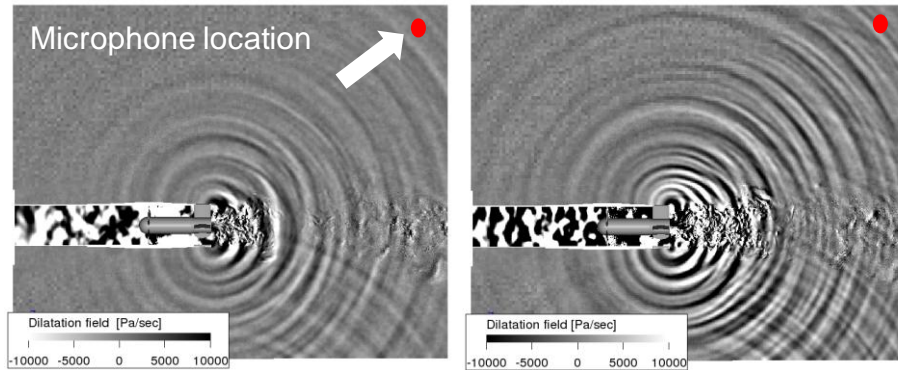


Figure 19: Instantaneous dilatation field for Q_1 (left) and Q_2 (right) using t_{c1}

B. Tip clearance effect

Increasing the tip clearance has a significant effect on the flow structures. As shown in Figure 20, the smaller tip clearance tends to accelerate the flow in the blade/hub area, causing a larger detachment and therefore higher local noise level generation especially at low frequencies (as confirmed in Figure 22). An interesting aspect observed in Figure 21 is the tip vortex level of coherence related to the tip clearance size. For a smaller tip clearance, the tip vortex is not coherent, resulting in numerous turbulent structures which are quickly dissipated via vortex-to-vortex interaction. This type of dissipation is very often associated to noise generation. With larger tip clearance, the tip vortex is much more coherent. The vortex is convected further downstream and is slowly dissipated via viscous mechanism. Such a mechanism is known to generate little or no noise. These observations are confirmed by the wall-pressure fluctuations in Figure 22 as the hub/blade area fluctuations are higher with a smaller tip clearance while the tip area is a major source of fluctuations especially at high frequencies, corresponding to the tip vortex structure breakdown mentioned earlier.

Overall, a smaller tip clearance will result in higher noise levels, as confirmed by the dilatation field observed in Figure 23.

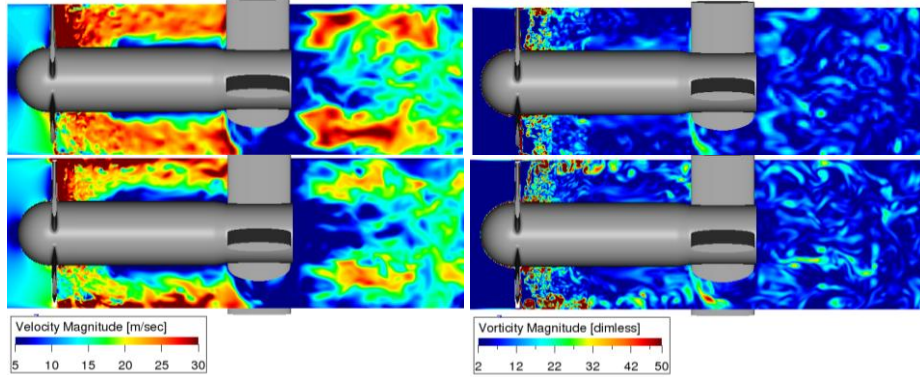


Figure 20: Instantaneous velocity magnitude (left) and vorticity magnitude (right). Top: Tip clearance ratio t_{c1} ; Bottom: t_{c2}

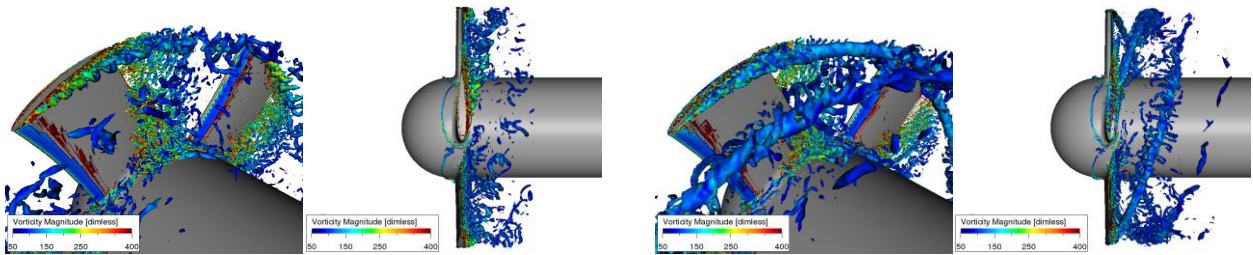


Figure 21: Instantaneous Isosurface of λ_2 colored by vorticity magnitude; (left) t_{c1} ; (right) t_{c2}

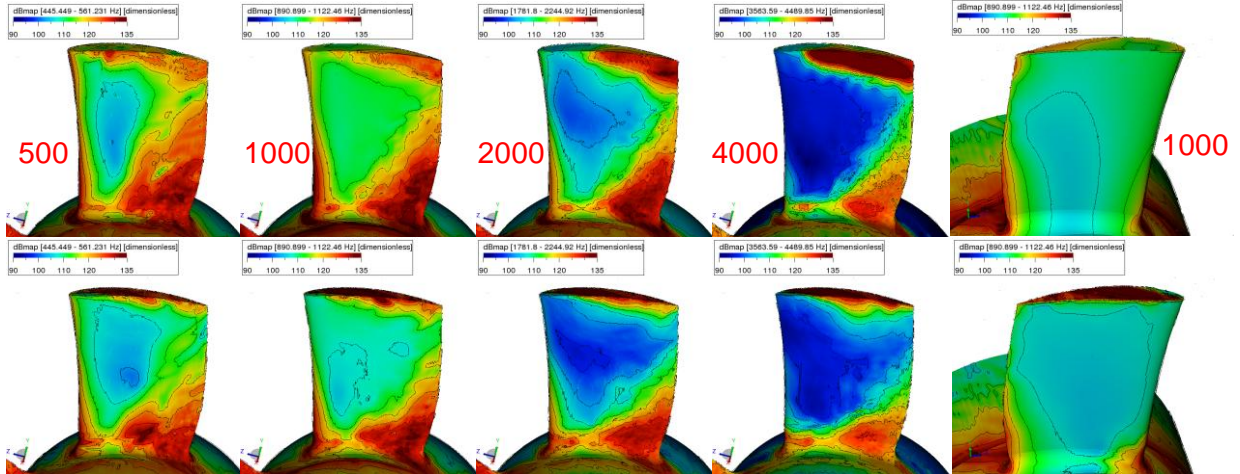


Figure 22: Surface dBmaps. (left) suction side for frequencies 500 to 4000Hz; (right) pressure side for 1000Hz third octave band; (top) t_{c1} ; (bottom) t_{c2}

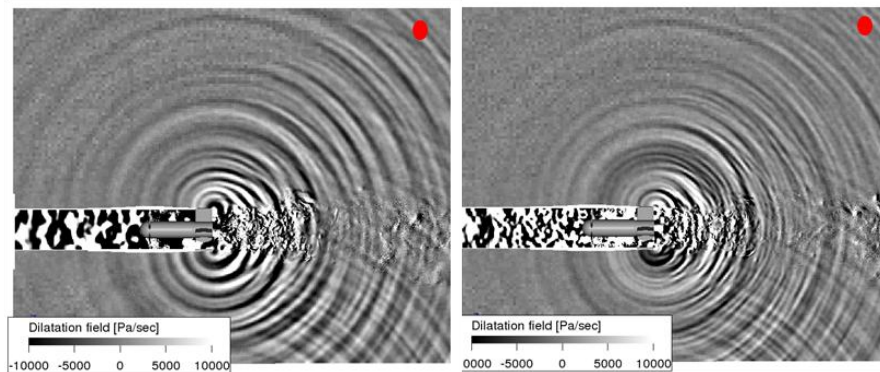


Figure 23: Instantaneous dilatation field for t_{c1} (left) and t_{c2} (right)

VI. Conclusion

In this paper, a numerical approach to simulate direct aeroacoustics contributions of a Wells Turbine is investigated and compared to experimental measurements. Simultaneous flow and acoustics predictions are obtained using a LBM-VLES method, with the real rotation of the fan implemented. The numerical results favorably compare to experiments for both pressure drop and torque predictions. The overall SPL radiated by the turbine is also shown to be in very good agreements with measurements. The simulation is used to investigate the instantaneous flow topology and to expose the link between flow structures and noise generation. It is suggested that the flow detachment on the suction side of the blades and the tip vortex are strong noise source candidates. The tip vortex seems to be the main contributor to high frequency content while the flow detachment close to the hub area contributes over the whole range of studied frequencies. The tip clearance size effect is also numerically investigated and compared to experiments. Increasing the tip clearance leads to low aerodynamic performances. However, the noise levels are not degraded in the optimum operation condition and are reduced in the second operating point. The numerical analysis shows how the tip clearance size impacts the flow around the rotor, especially on the coherence of the tip vortex as well as on the intensity of the flow detachment. The flow structures correlation with wall pressure fluctuations and propagated noise is also investigated. Further studies concerning stall regime and blade design modifications will be presented in the future.

References

- ¹Starzmann, R.: Aero-Acoustic Analysis of Wells Turbines for Ocean Wave Energy Conversion. Fortschritt-Bericht VDI Reihe 7 Nr. 500, VDI-Verlag, 2012 (PH.D. thesis University of Siegen, Germany).
- ²Raghunathan, S., Tan, C. P., Ombaka, O. O., 1985, "Performance of the Wells self-rectifying air turbine", *Aeronautical Journal*, 89(890), pp. 369-379.
- ³Raghunathan, S., Ombaka, O. O., 1985, "Effect of frequency of air flow on the performance of the Wells turbine", *International Journal of Heat and Fluid Flow*, 6(2), pp. 127-132.
- ⁴Koch, S., 2009, "Entwicklung eines Steuerungssystems und einer Messwerterfassung für einen Turbinenprüfstand", Studienarbeit Nr. A09-2/1 am Institut für Fluid- und Thermodynamik, Universität Siegen, Germany.
- ⁵Gerik, M., 2011, "Experimentelle Untersuchung der Strömung in einem Wellsturbinen Prüfstand", Studienarbeit Nr. A09-2/6 am Institut für Fluid- und Thermodynamik, Universität Siegen, Germany.
- ⁶Frisch, U., Hasslacher, B. and Pomeau, Y., 1986, "Lattice-gas Automata for the Navier-Stokes Equations", *Phys. Rev. Lett.*, Vol. 56, pp.1505-1508.
- ⁷Chen, H., Chen, S., and Matthaeus, W., "Recovery of the Navier-Stokes equations using a lattice-gas Boltzmann method", *Phys.Rev. A* 45, 5339-5342 (1992).
- ⁸Chen, H., Teixeira, C. and Molvig, K., "Digital physics approach to computational fluid dynamics: Some basic theoretical features", *Intl. J. Mod. Phys. C* 9 (8), 675 (1997).
- ⁹Chen, H., Teixeira, C., Molvig, K., "Realization of Fluid Boundary Conditions via Discrete Boltzmann Dynamics," *Intl J. Mod. Phys. C*, Vol. 9 (8), pp. 1281-1292, 1998.
- ¹⁰Thantanapally, C., Singh, S., Succi, S., and Ansumali, S., "Quasi-equilibrium lattice Boltzmann models with tunable Prandtl number for incompressible hydrodynamics", *International Journal of Modern Physics C* 24 (12), 1340004 (2013).
- ¹¹Chen, H., "Volumetric Formulation of the Lattice Boltzmann Method for Fluid Dynamics: Basic Concept", *Phys. Rev. E*, Vol. 58, pp. 3955-3963, 1998.
- ¹²Shan, X. and Chen, H., "A general multiple-relaxation-time Boltzmann collision model", *International Journal of Modern Physics C* 18, 635 (2007).
- ¹³Chen, H., Goldhirsh, I., Orszag, S., "Discrete rotational symmetry, moment isotropy, and higher order lattice Boltzmann models" *J. Sci. Computing*, submitted (August. 2007).
- ¹⁴Bhatnagar, P., Gross, E. and Krook, M., 1954, "A model for collision processes in gases. I. small amplitude processes in charged and neutral one-component system", *Pys. Rev.*, vol.94, pp.511-525, 1954.
- ¹⁵Chapman, S. and Cowling, T., "The Mathematical Theory of Non-Uniform Gases", Cambridge University Press, 1990.
- ¹⁶Yakhot, V., "Extended Boltzmann Kinetic Equation for Turbulent Flows", *Science*, Vol. 301, pp. 633-636, 2003.
- ¹⁷Shan, X. and Chen, H., 1993, "Lattice Boltzmann model for simulating flows with multiple phases and components", *Phys. Rev. E*, 47, 1815-1819.
- ¹⁸Li, Y., Shock, R., Zhang, R., and Chen, H., 2004, "Numerical Study of Flow Past an Impulsively Started Cylinder by Lattice Boltzmann Method" *J. Fluid Mech.*, Vol. 519, pp. 273-300.
- ¹⁹Chen, H., Kandasamy, S., Orszag, S., Shock, R., Succi, S. and Yakhot, V., "Extended Boltzmann Kinetic Equation for Turbulent Flows", *Science*, Vol. 301, pp. 633-636, 2003.
- ²⁰Chen, H., Orszag, S., Staroselsky, I. and Succi, S., 2004, "Expanded Analogy between Boltzmann Kinetic Theory of Fluid and Turbulence", *J. Fluid Mech.*, Vol. 519, pp. 307-314.
- ²¹B. Crouse, G. Balasubramanian, S. Senthoooran, D. Freed, K.D. Ih, and S.R. Shin, Investigation of Gap Deflector Efficiency for Reduction of Sunroof Buffeting, SAE conference 2009-01-2233.

²²F. Pérot, M. Meskine, and S. Vergne, “Investigation of the Statistical Properties of Pressure Loadings on Real Automotive Side Glasses”, AIAA paper 2009-3402, 13th AIAA/CEAS aeroacoustics conference, Miami, Florida, 2009.

²³S. Senthoooran, B. Crouse, G. Balasubramanian, D. Freed, S.R. Shin and K.D. Ih, “Effect of Surface Mounted Microphones on Automobile Side Glass Pressure Fluctuations”, Proc. 7th MIRA Intl. Vehicle Aerodynamics Conf., Richoh Arena, UK, Oct.22, 2008.

²⁴J.L. Adam, D. Ricot, F. Dubief, and C. Guy, “Aeroacoustic Simulation of Automotive Ventilation Outlets”, Proc. Acoustics 08 Conference., Paris, June 29, 2008.

²⁵Pérot, F., Kim, M.S., D.M. Freed , Dongkon, L., Ih, K.D., Lee, M.H., 2010a, “Direct aeroacoustics prediction of ducts and vents noise”, AIAA paper 2010-3724, 14th AIAA/CEAS aeroacoustics conference, Stockhlo, June.

²⁶A. Laffite, F. Pérot, “Investigation of the Noise Generated by Cylinder Flows Using a Direct Lattice-Boltzmann Approach”, AIAA 2009-3268, 13th AIAA/CEAS aeroacoustics conference, Miami, Florida, 2009.

²⁷G.A. Brès, F. Pérot, D. Freed, “Properties of the Lattice-Boltzmann Method for Acoustics”, AIAA 2009-3395, 13th AIAA/CEAS aeroacoustics conference, Miami, Florida, 2009.